Low-Symmetry Diffusion Barriers in Homoepitaxial Growth of Al(111)

Alexander Bogicevic, Johan Strömquist, and Bengt I. Lundqvist
Department of Applied Physics, Chalmers University of Technology and Göteborg University, S-412 96 Göteborg, Sweden
(Received 22 October 1997)

From fractals to compact islands, epitaxial growth offers an exotic variety of surface morphologies that emanate from a handful of elementary atomic diffusion processes. Adsorption calculations have hitherto been limited to high-symmetry configurations, or to semiquantitative methods. Using extensive density-functional calculations on parallel computers we map out barriers for self-diffusion at steps, kinks, and corners on Al(111). The results reveal an unexpected exchange diffusion mechanism at kinks and a large anisotropy at corners, and are used to predict various growth modes. [S0031-9007(98)06653-8]

PACS numbers: 68.55.–a, 66.30.Fq, 68.35.Fx, 68.60.–p

The empirical approach in man's ways of making materials—documented as early as 4000 years ago in, e.g., the Sumerian culture—is now successively being supplemented by methods such as chemical vapor deposition, molecular beam epitaxy, and in detail monitored metallurgical processes, based on an atomic-scale point of view: materials are made atom by atom [1]. Growth of materials depends ultimately on bonding and motion of individual atoms and clusters of atoms on surfaces. During growth an atom can undergo a number of different *elementary processes*. Each process is characterized by delicate energy parameters for bonding and diffusion, and the integrated effect of all of these processes is the growth. This Letter provides an extensive mapping of such processes and their relevant energies. It also draws some immediate consequences about growth modes.

The first step towards a detailed understanding of surface morphology during and after growth is to map out all relevant atomic processes, such as terrace diffusion, corner crossing, and kink breaking (Fig. 1). Experimental techniques such as field ion (FIM) and scanning tunneling microscopy (STM) help to ascertain that no diffusion processes are left out [1].

The next step is to determine the rates for all processes. For each atomic process i, one has to find the activation energy E_i and the corresponding prefactor ν_i^0, yielding a collection of rates $\{\nu_i\}$ given by (transition state theory [2])

$$\nu_i = \nu_i^0 e^{-E_i/k_B T}, \tag{1}$$

where k_B is the Boltzmann constant and T is the substrate temperature.

The final step is to realize that, as the temperature is increased, more and more of these processes become activated. Once all relevant diffusion processes are identified and their rates are determined, the morphology evolution of a surface during and after growth can be calculated with a kinetic Monte Carlo (KMC) algorithm that yields the evolution of all atoms in the system on laboratory time and size scales. Such lattice-gas simulations have been implemented to study crystal growth of metals [3–5] and semiconductors [6–8], and are for this purpose superior to conventional molecular dynamics and Monte Carlo methods that cannot probe sufficiently long time scales.

The most fragile link in this three-step approach is the determination of process rates. Direct experiments offer some help, but it is hard to resolve and monitor a large set of intricate processes even with atomic-resolution tools such as FIM and STM. Still, input rates have often been extracted indirectly from STM studies of island densities [3–5], and treated as effective parameters. A large variety of surface phenomena have been subject to theoretical studies using rates calculated from simple bond-counting models or semiempirical and quasiclassical methods [9–11], such as the embedded atom method [12] and the effective medium theory (EMT) [13]. Unfortunately, such methods do not sufficiently account for important quantum-mechanical effects [14] and frequently lack the necessary resolution needed for even a qualitative understanding of growth phenomena.

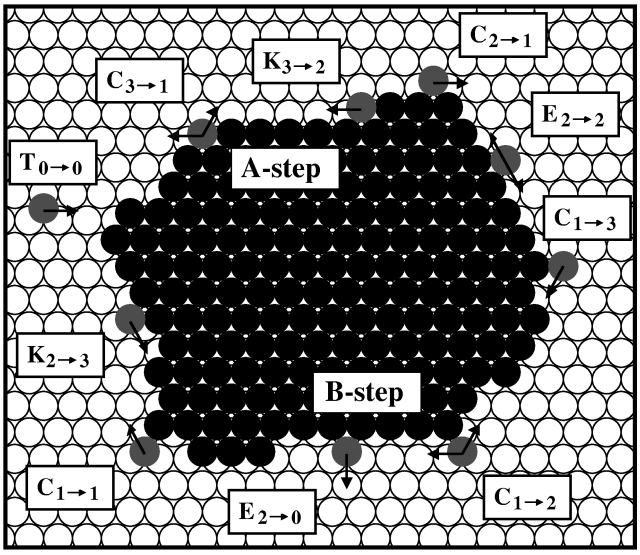

FIG. 1. Illustration of the diffusion processes considered in this study. All processes can take place on both *A* and *B* steps. The notation is described in the text.

The best and most accurate solution to this problem is offered by density-functional theory (DFT) [15,16]. Unfortunately, the formidable computational effort associated with such calculations has hitherto very effectively kept the number of diffusion studies down and limited them to configurations of high symmetry, such as straight steps. Since real growth conditions involve far more irregular clusters than just straight steps, it is of fundamental importance to accurately investigate also low-symmetry processes, and assess more approximate and indirect methods.

Here we provide an extensive set of accurate values for diffusion barriers of elementary diffusion processes fundamental to growth morphology. We examine the self-diffusion around steps, corners, and kinks for Al(111), and present energy barrier values for more than a dozen diffusion processes beyond the previously considered ones at straight steps (which we also consider in detail). We proceed by making a first estimate on what influence these barriers will have in different stages of growth.

The needs for considering low-symmetry configurations are manyfold. For instance, at low temperatures, diffusion around corners determines the randomness and compactness of fractal atom aggregates [17], and at high temperatures kink and corner breaking induce a transition towards equilibrium-shaped compact islands [9] and lead to island migration by periphery diffusion [11,18]. Aluminum is chosen for this study since it is a prototype of a simple s-p metal, and hopefully the interpretations of the results can be transferred to other systems. Naturally, we benefit from the relatively simple electron structure which lowers the calculational demands.

We use DFT [15,16] in a pseudopotential plane-wave method [19], applying both the local density (LDA) [20] and generalized gradient approximation (GGA) [21] for the exchange-correlation functional. This approach encompasses all quantum-mechanical effects relevant for adsorption to a high level of accuracy. The LDA calculations are performed self-consistently, whereas the semilocal exchange-correlation corrections of the GGA are calculated from LDA densities, so-called post-GGA. Extensive self-consistent calculations within the GGA have shown this to be an excellent approximation due to the variational property of the total energy functional [21,22]. The numerical accuracy is carefully controlled by extensive k-point summation (all values are calculated using 2, 4, 8, and sometimes 16 k-points) at an energy cutoff of 9 Ry, using large supercells (109–192 atoms with >11 Å of vacuum). The Kohn-Sham equations are solved by alternating conjugate gradient minimizations and subspace rotations, while simultaneously optimizing the atomic structure using damped dynamics. The results presented in this study are based on calculations that have taken a time equivalent to over 11 years of CPU time on a fast workstation such as the Sun Ultra-2.

In the following discussion, it is important to realize that the smooth (111) surface hosts two types of close-packed steps, the B step with a $\{111\}$ microfacet and the A step with a more open $\{100\}$ microfacet [23] (see Fig. 1). Experimentally, it has been shown for several materials how these two types of steps behave rather differently during growth [23–25]. We will show here how the different geometries of the two types of steps lead to different diffusion barriers and sometimes to different diffusion mechanisms.

The diffusion processes regarded here are illustrated schematically in Fig. 1, and the respective activation barriers are summarized in Table I. Each process is characterized by a letter (T for terrace, E for edge, K for kink, and C for corner) and a subscript that indicates the number of in-layer nearest neighbors before and after the jump. All barriers are given in eV as calculated within LDA/GGA, and n_i indicates the number of Al atoms in the supercell. In the following, we highlight some of the results presented in Table I.

(i) Edge diffusion has previously been found to proceed by an exchange mechanism at B steps and by regular hopping along A steps [14]. This step-type dependence of the diffusion mechanism at edges is expected to be found for kink breaking ($K_{3\to2}$) and kink incorporation ($K_{2\to3}$), as well. Accordingly, we find these processes to proceed by exchange at B steps. What is more surprising is that the exchange mechanism is operative also at A steps. Exchange is favored over hopping by 0.06–0.07 eV in the GGA.

(ii) We find a strong anisotropy in corner diffusion ($C_{1\to2}$), with an energy barrier to B steps that is 400% larger than to A steps. This is an important result as the anisotropy controls the growth mode at low temperatures (see below). We note that the barriers are practically unaffected by the corner angle ($\pi/3$ or $2\pi/3$). Previous efforts to find this effect using EMT have shown varying magnitude and direction of anisotropy with system [9,17,26].

(iii) The reverse process of corner crossing ($C_{2\to1}$) has an activation barrier that is almost independent of step

TABLE I. Activation energies in eV for a set of elementary diffusion processes as calculated within the LDA/GGA. The processes are designated by a letter, T for terrace, E for edge, K for kink, C for corner, and a subscript that shows the number of in-layer nearest neighbors before and after the jump. A comparison to the few earlier calculated results is also shown (minor deviations are partly attributed to the larger energy cutoff and k-point sampling used here).

Process	n_i	$\Delta E^A_{\rm hop}$	$\Delta E^A_{\rm exc}$	$\Delta E^B_{\rm hop}$	$\Delta E^B_{\rm exc}$
$E_{2\to2}$	109–190	0.31/0.31	0.43/0.36	0.45/0.45	0.35/0.26
	Ref. [14]	0.32	0.44	0.48	0.39–0.42
$K_{3\to2}$	135–192	0.47/0.45	0.46/0.38	0.67/0.65	0.49/0.42
$K_{2\to3}$	135–192	0.27/0.28	0.26/0.22	0.41/0.42	0.24/0.19
$C_{1\to1}$	129	0.18/0.18		0.22/0.22	
$C_{1\to2}$	129	0.04/0.05		0.17/0.19	
$C_{2\to1}$	129	0.33/0.33		0.32/0.30	
$C_{3\to1}$	131	0.62/0.59		0.63/0.60	
$C_{1\to3}$	131	0.03/0.04		0.14/0.14	

type (A or B), and the same is true for corner breaking ($C_{3\to1}$). Corner flipping ($C_{1\to1}$) has a slightly lower barrier at A steps than at B steps.

The calculated catalog of energies is presently being used in KMC simulations of epitaxial growth [27]. Already here, however, a valuable positioning of the various atomic processes on the temperature scale can be made together with rough growth mode estimates. Since prefactors, in general, do not vary much with diffusion process (or material) [28], and enter the rate equation only linearly, we focus on the activation energies that exponentially control the diffusion rates through Eq. (1).

Using Eq. (1), we can define an activation temperature T_i at which each process i is considered activated, i.e., takes place at a rate Γ:

$$T_i = \frac{E_i/k_B}{\ln(\nu^0/\Gamma)}. \quad (2)$$

We use $\nu^0 = 6 \times 10^{12}$ (calculated within the harmonic approximation for kink breaking) for all processes i. The value of Γ depends on the experimental growth rate. We choose a typical value $\Gamma = 1\ \mathrm{s}^{-1}$ [14], relevant for a deposition rate of about 0.001–0.1 ML/s (similar estimates can be obtained from the ratio of deposition rate to average island density [29]). We note that even if we change our definition of Γ or the prefactor ν^0 by a factor of 10, the activation temperatures will change by less than 10% due to the logarithmic way in which these rates enter Eq. (2). Figure 2 illustrates how an increasing number of atomic processes are activated as the temperature grows.

0–70 K.—Already around 17 K, terrace diffusion ($T_{0\to0}$) is activated (dimers can at this temperature rotate within a hexagonal cell of six sites, but cannot leave the cell until around 51 K, and then by concerted sliding [30]). This low-temperature activation might seem ideal for observing classical diffusion-limited aggregation (DLA), where fractals grow by a hit-and-stick mechanism. In such a scenario, only terrace diffusion is activated, and atoms diffuse around on the surface until they irreversibly attach to the perimeter of a growing atom aggregate, resulting in so-called purely fractal growth [17,25]. This is, however, not the case here since corner diffusion to A steps ($C^A_{1\to2}$) is activated as soon as terrace diffusion sets in (Fig. 2). This anisotropic corner diffusion (the same process to B steps is activated at higher temperatures) induces for most deposition rates so-called dendritic growth [17,25], where ramified fractals grow in three preferential directions. Hence, dendritic growth should prevail already at low temperatures.

The similar anisotropy found for corner incorporation ($C_{1\to3}$) has negligible impact in this temperature regime since the islands are not compact. This mechanism is, hence, rarely operative. When going to three instead of two neighbors ($C_{1\to2}$), the barriers are lowered just slightly, in line with our expectations above.

Another effect of corner diffusion is to slightly increase the width of the fractal "arms" [3,31]. In a recent Letter [17], Brune and co-workers propose a multistep mechanism for the growth of (more than one-atom wide) dendrites. One link in this approach is the assumption that corner flipping ($C_{1\to1}$) is activated at much lower temperatures than corner diffusion to B steps ($C^B_{1\to2}$). Since this is not the case for our system (both processes are activated at around 70–80 K), we conclude that the proposed mechanism is not general.

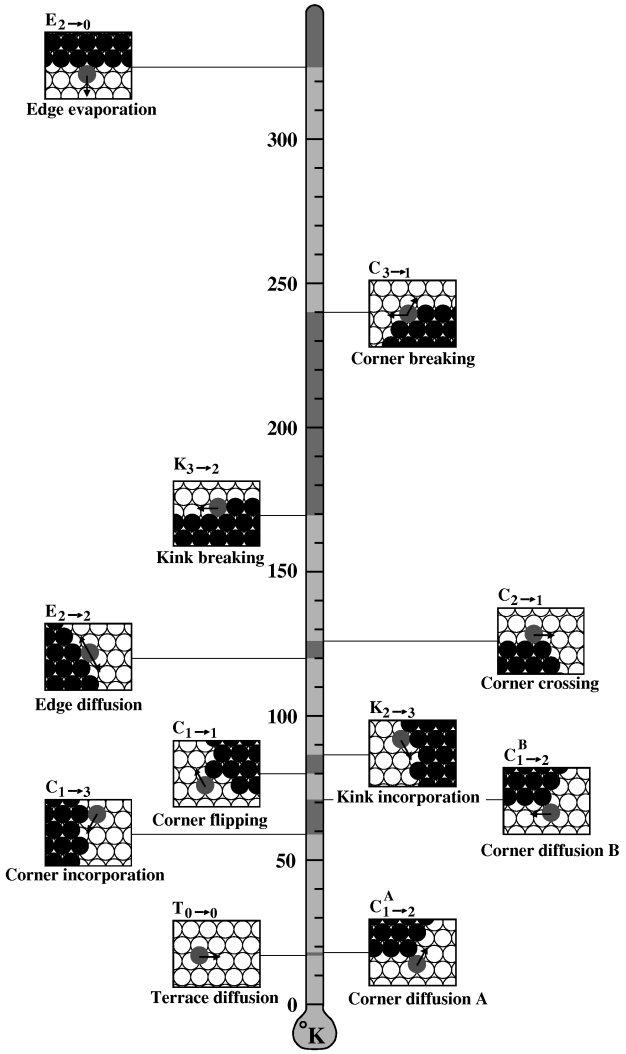

FIG. 2. Temperature scale of Al(111) homoepitaxy with calculated onsets [Eq. (2)] of elementary atomic diffusion processes.

70–120 K.—As corner diffusion to B steps ($C^B_{1\to2}$) becomes activated at around 70 K, while edge diffusion ($E_{2\to2}$) and corner crossing ($C_{2\to1}$) are frozen, we expect a gradual transition towards less pronounced dendrites with increasing temperature. At 71–75 K (87 K) the corner flipping process ($C_{1\to1}$) at A (B) steps is activated as well. Terrace atoms that happen to attach next to a kink site are effectively incorporated into the kink ($K_{2\to3}$) at around 71–98 K (GGA and LDA values differ somewhat).

120–170 K.—As the temperature is increased above 118–122 K, we expect a transition to compact islands induced by edge diffusion and corner crossing processes.

The edge atoms are now free to diffuse along the steps and cross corners until they are captured by a kink ($K_{2\to3}$). The origin of the transitions in compact growth shapes observed in homoepitaxial growth of Pt(111) [24] is still debated, and to avoid further confusion, we choose to comment on this subject for Al(111) in a forthcoming report based on KMC simulations [27].

170–325 K.—When the temperature reaches $\simeq$157–189 K, kink atoms begin breaking away ($K_{3\to2}$), and around 232–248 K corner breaking ($C_{3\to1}$) is activated. These processes induce a transition towards islands with equilibrium shapes of rounded hexagons [31]. Furthermore, the activation of kink and corner breaking induces island migration by periphery diffusion [11,32,33].

As the temperature goes up and the kinetic energy of a diffusing particle reaches a substantial fraction of the potential energy barrier, the diffusion becomes more (2D) liquidlike and proceeds no longer via simple hops between fcc and hcp sites. If we assume that this starts happening when the kinetic energy is roughly half the diffusion barrier, we predict substantial off-site terrace diffusion and corner diffusion to A steps for $T > 250$ K.

>325 K.—At around 325 K, edge evaporation ($E_{2\to0}$) is activated (the barrier being $\simeq$0.8 eV), and neighboring islands exchange atoms. This evaporation-condensation mechanism will add to the existing island mobility [32,33], and induce Ostwald ripening [34,35].

In summary, we present accurate density-functional calculations of low-symmetry diffusion barriers fundamental to epitaxial growth of Al(111) and predict various growth modes that should be observed at given temperatures. These results are essential input in kinetic Monte Carlo simulations of growth, and constitute a reference frame for more approximate methods.

We are indebted to Horia Metiu for introducing us to the subject of growth, and thank him, Joachim Jacobsen, and Harald Brune for valuable discussions. Financial support through the Materials Consortium No. 9, supported by the Swedish Board for Industrial and Technical Development (NUTEK) and the Swedish Foundation for Strategic Research (SSF), the Swedish Natural Science Research Council (NFR), and the Swedish Research Council for Engineering Sciences (TFR), together with allocation of time on the SGI supercomputer on the Chalmers campus are gratefully acknowledged.

Note added.—Following the submission of this manuscript, a new STM study by Fischer *et al.* [36] was performed on the Al/Al(111) system that very nicely indicates the high accuracy and predictive power of our method: (A) Our prediction of dendrites (rather than fractals) at low temperatures is confirmed by measurements at 60-100 K. (B) We foresee a transition to compact islands at 118-122 K, in excellent agreement with the experimentally observed transition at 120 K. (C) Our prediction of a transition to hexagonal islands near 200 K is confirmed experimentally (transition at 200 K). (D) Our terrace diffusion barrier of 0.04 eV is in good agreement with the experimental value of 0.042 ± 0.005 eV. The overall excellent agreement indicates a good choice of onset rate Γ. We also note the good agreement with the few earlier calculated DFT-LDA barrier values [14] (Table I). During the time of the manuscript refereeing period, we have performed full kinetic Monte Carlo simulations at low to intermediate temperatures ($T = 30$-140 K) for a large array of deposition rates ($F = 10^{-6}$–1 ML/s), using the activation energies reported in this manuscript [27]. We find that the transition to compact islands occurs at 120 K for $F = 10^{-4}$ ML/s, and at about 130-140 K for $F = 10^{-3}$ – 10^{-2} ML/s. This is within 10–20 K of what our simplified approach above predicts, in pleasingly good agreement with this approach and the experimental data.

[1] M. G. Lagally, Phys. Today **46**, 24 (1993).
[2] P. Hänggi *et al.*, Rev. Mod. Phys. **62**, 251 (1990).
[3] Z. Zhang *et al.*, Phys. Rev. Lett. **73**, 1829 (1994).
[4] J. G. Amar and F. Family, Phys. Rev. Lett. **74**, 2066 (1995).
[5] M. C. Bartelt *et al.*, Phys. Rev. Lett. **75**, 4250 (1995).
[6] S. V. Ghaisas *et al.*, Phys. Rev. Lett. **56**, 1066 (1986).
[7] S. Clarke *et al.*, Phys. Rev. Lett. **58**, 2235 (1987).
[8] H. Metiu *et al.*, Science **255**, 1088 (1992).
[9] J. Jacobsen *et al.*, Phys. Rev. Lett. **74**, 2295 (1995).
[10] Z.-P. Shi *et al.*, Phys. Rev. Lett. **76**, 4927 (1996).
[11] A. Bogicevic, S. Liu, J. Jacobsen, B. I. Lundqvist, and H. Metiu, Phys. Rev. B **57**, 4289 (1998).
[12] M. S. Daw *et al.*, Phys. Rev. Lett. **50**, 1285 (1983).
[13] K. W. Jacobsen *et al.*, Phys. Rev. B **35**, 7423 (1987).
[14] R. Stumpf and M. Scheffler, Phys. Rev. Lett. **72**, 254 (1994); Phys. Rev. B **53**, 4958 (1996).
[15] P. Hohenberg and W. Kohn, Phys. Rev. **136**, B864 (1964).
[16] W. Kohn and L. J. Sham, Phys. Rev. **140**, A1133 (1965).
[17] H. Brune *et al.*, Nature (London) **369**, 469 (1994); Surf. Sci. Lett. **349**, L115 (1996).
[18] J. W. Evans, P. A. Thiel, and R. Wang (to be published).
[19] B. Hammer, computer code DACAPO version 1.18, CAMP, Denmark Technical University.
[20] J. P. Perdew *et al.*, Phys. Rev. B **23**, 5048 (1981).
[21] J. P. Perdew *et al.*, Phys. Rev. B **46**, 6671 (1992).
[22] B. Hammer *et al.*, Phys. Rev. Lett. **70**, 3971 (1993).
[23] S. C. Wang *et al.*, Phys. Rev. Lett. **67**, 2509 (1991).
[24] T. Michely *et al.*, Phys. Rev. Lett. **70**, 3943 (1993).
[25] M. Hohage *et al.*, Phys. Rev. Lett. **76**, 2366 (1996).
[26] J. Jacobsen *et al.* (to be published).
[27] A. Bogicevic (to be published).
[28] C. L. Liu *et al.*, Surf. Sci. **253**, 334 (1991).
[29] M. C. Bartelt and J. W. Evans, Surf. Sci. Lett. **314**, L829 (1994).
[30] A. Bogicevic, P. Hyldgaard, G. Wahnström, and B. I. Lundqvist, Phys. Rev. Lett. **81**, 172 (1998).
[31] J. Jacobsen *et al.*, Surf. Sci. **359**, 37 (1996).
[32] J. M. Wen *et al.*, Phys. Rev. Lett. **76**, 652 (1996).
[33] D. S. Sholl *et al.*, Phys. Rev. Lett. **75**, 3158 (1995).
[34] W. Ostwald, Z. Phys. Chem., Leipz. **34**, 495 (1900).
[35] G. S. Bales *et al.*, Phys. Rev. B **50**, 6057 (1994).
[36] B. Fischer, J. Weckesser, J. Barth, H. Brune, and K. Kern (to be published).